Efficiency improvement of dye-sensitized solar cells using graft copolymer-templated mesoporous TiO₂ films as an interfacial layer

Sung Hoon Ahn, Harim Jeon, Kyung Jin Son, Hyungju Ahn, Won-Gun Koh, Du Yeol Ryu and Jong Hak Kim*

Organized mesoporous TiO₂ films with high porosity and good connectivity were synthesized *via* sol–gel by templating an amphiphilic graft copolymer consisting of poly(vinyl chloride) backbone and poly(oxyethylene methacrylate) side chains, *i.e.*, PVC-*g*-POEM. The randomly microphase-separated graft copolymer was self-reorganized to exhibit a well-ordered micellar morphology upon controlling polymer–solvent interactions, as confirmed by atomic force microscope (AFM) and glazing incidence small-angle X-ray scattering (GISAXS). These organized mesoporous TiO₂ films, 550 nm in thickness, were used an an interfacial layer between a nanocrystalline TiO₂ thick layer and a conducting glass in dye-sensitized solar cells (DSSC). Introduction of the organized mesoporous TiO₂ layer resulted in the increased transmittance of visible light, decreased interfacial resistance and enhanced electron lifetime. As a result, an energy conversion efficiency of DSSC employing polymer electrolyte was significantly improved from 3.5% to 5.0% at 100 mW cm⁻².

Introduction

Dye-sensitized solar cells (DSSCs) have received attention recently due to their low cost and high efficiency, and have been perceived as a good alternative to silicon solar cells since they were first proposed by the Grätzel group in 1991.[1] DSSCs consist of a dye-sensitized mesoporous TiO₂ layer, a Pt layer, and an electrolyte containing a redox couple. An energy conversion efficiency of 11% has been achieved in DSSCs with an organic liquid-based electrolyte containing I_3^-/I^- as a redox couple.[2] The performances of DSSCs can be improved by developing, modifying or improving any of the following: the dye,[2,3] the nanocrystalline TiO₂ layer,[4,5] the thermal-resistance transparent conducting oxide (TCO),[6] the electrolyte[7,8] or the electrode–electrolyte interface.[9,10] In particular, controlling the structure of the TiO₂ films plays a crucial role in determining the energy conversion efficiency of DSSCs because it influences the quantity of dye adsorbed and the electron transport. Thus, much prior research has focused on the relationship between nanocrystalline TiO₂ structure and energy conversion efficiency.[11–16]

In general, porous nanocrystalline TiO₂ films have been prepared by a colloid solution where the TiO₂ nanoparticles are dispersed in a solvent. However, incomplete dispersion and aggregation of particles frequently cause poor interfacial contact between the TiO₂ layer and the TCO layer, leading to poor electron transfer. One of the methods for enhancing interfacial properties is introducing a thin interfacial (or buffer) layer between the thick nanocrystalline TiO₂ layer and the TCO layer.[17–19] For example, organized mesoporous TiO₂ thin films have been utilized as an interfacial layer, which results in an improvement in energy conversion efficiency due to increased

transmittance of visible light and better adhesion between the SnO₂/F-layered conductive glass (FTO) and the main TiO₂ layer.[20–23]

In general, organized mesoporous TiO₂ films have been synthesized *via* a sol–gel process using an amphiphilic block copolymer, *e.g.*, a poly(ethylene oxide) (PEO)-based template.[24–30] For example, Coakley *et al.*[24] prepared porous TiO₂ films with a uniform pore size and without any aggregation of the particles using a Pluronic poly(ethylene oxide)-*b*-poly(propylene oxide)-*b*-poly(ethylene oxide) (PEO-*b*-PPO-*b*-PPO) triblock copolymer (P123) as a structure-directing agent. Our group recently synthesized organized mesoporous TiO₂ films using an amphiphilic graft copolymer consisting of poly(vinyl chloride) backbone and poly-(oxyethylene methacrylate) side chains, *i.e.*, PVC-*g*-POEM,[31] which is more attractive than block copolymers due to its low cost and facile synthetic method.[32,33] As a result, a solid-state DSSC employing the organized 700 nm thick TiO₂ film exhibited a solar conversion efficiency of 2.2% at 100 mW cm⁻², which was approximately two-fold higher than that attained from a DSSC employing a random TiO₂ film.[31]

In this work, microphase-separated PVC-*g*-POEM graft copolymer with a well-ordered micellar morphology was templated to synthesize organized mesoporous TiO₂ films *via* a sol–gel process which involved controlling polymer–solvent interactions. Synthesized films were characterized in detail by atomic force microscopy (AFM) and glazing incidence small-angle X-ray scattering (GISAXS). In particular, organized TiO₂ thin films with different porosity and pore size were prepared by carefully changing the mole ratio of [TTIP]:[H₂O]:[HCl]. The organized TiO₂ thin films were utilized as an interfacial layer in DSSCs and the influence of the material structure on photovoltaic performance was investigated. Detailed properties of materials were systematically characterized using scanning electron microscopy (SEM), non-contact three-dimensional (3D) surface profilometry and electrochemical impedance spectroscopy (EIS).

Department of Chemical and Biomolecular Engineering, Yonsei University, 262 Seongsanno, Seodaemun-gu, Seoul, 120-749, South Korea. E-mail: jonghak@yonsei.ac.kr; Fax: +82-2-312-6401; Tel: +82-2-2123-5757

Experiment

Materials

Poly(vinyl chloride) (PVC, M_w = 97 000 g mol^{-1}, M_n = 55 000 g mol^{-1}), poly(oxyethylene methacrylate) (POEM, poly(ethylene glycol) methyl ether methacrylate, M_n = 475 g mol^{-1}), titanium(IV) isopropoxide (TTIP, 97%), hydrogen chloride solution (HCl, 37 wt%), 1,1,4,7,10,10-hexamethyltriethylene tetramine (HMTETA, 99%), and copper(I) chloride (CuCl, 99%), fumed silica nanoparticles (SiO$_2$, 14 nm), poly(ethylene glycol dimethyl ether) (PEGDME, M_n = 500 g mol^{-1}) and iodine (I$_2$) were purchased from Aldrich. 1-Methyl-3-propyl imidazolium iodide (MPII, C$_7$H$_{13}$N$_2$I) and ruthenium dye (535-bisTBA, N719) were purchased from Solaronix, Switzerland. Tetrahydrofuran (THF), N-methyl pyrrolidone (NMP), and methanol were obtained from J. T. Baker. All solvents and chemicals were reagent grade and used as received.

Synthesis of the graft copolymer

PVC (6 g) was dissolved in 50 mL of NMP by stirring at 90 °C for 4 h. After cooling the solution to room temperature, 15 g of POEM, 0.1 g of CuCl, and 0.23 mL of HMTETA were added to the solution. The green mixtures were stirred until homogeneous, and were purged with nitrogen for 30 min. The reaction was carried out at 90 °C for 18 h. After polymerization, the resultant mixtures were diluted with THF. After passing the solutions through a column with activated Al$_2$O$_3$ to remove the catalyst, the solutions were precipitated into methanol. The grafted copolymers were purified by dissolving in THF and reprecipitating into methanol three times. PVC-g-POEM graft copolymer with PVC:POEM = 4 : 6 wt% ratio was obtained in a powder form and dried in a vacuum oven overnight at room temperature.

Preparation of the mesoporous TiO$_2$ films

A series of samples was prepared by varying the mole ratio of [TTIP]:[H$_2$O]:[HCl] from 2 : 1 : 0, 2 : 0.5 : 0.5 to 2 : 1 : 1. A solution was prepared by slowly adding HCl (37 wt%) to TTIP under vigorous stirring. Additional DI water was slowly added to the TTIP solution. Separately, 0.05 g of PVC-g-POEM graft copolymer was dissolved in 1.5 mL of THF and added to 0.6 g of the TTIP/HCl/THF solution. These solutions were aged by stirring at ambient temperature for at least 3 h. The films were deposited onto a FTO conducting glass using a SMSS Delta 80BM spin coater at 1500 rpm for 30 s. Upon calcination at 450 °C for 30 min, the organic chemicals were completely removed to produce the mesoporous TiO$_2$ thin films. The dense TiO$_2$ film with 100 nm thickness was prepared using spin coating of titanium(IV) bis(ethyl acetoacetato) diisopropoxide solution (2 wt% in butanol) at 1500 rpm for 10 s, followed by calcination at 450 °C for 30 min.

Characterization

UV–vis spectroscopy was performed with a spectrophotometer (Shimadzu) in the range of 300 to 800 nm. Morphologies of the mesoporous TiO$_2$ films were observed using a field-emission scanning electron microscope (FE-SEM, SUPRA 55VP,

Germany, Carl Zeiss), and by a non contact 3D surface profiler (NANO View-E1000, Nanosystem). Tapping mode atomic force microscopy (TM-AFM) (Nanoscope IV, Digital Instruments) was used to examine the morphologies of TiO$_2$ films. Grazing-incidence small-angle X-ray scattering (GISAXS) experiments were performed at the 4C2 beamline in the Pohang Accelerator Laboratory (PAL), Pohang, Korea. The operating conditions were set to a wavelength of 0.138 nm and a sample-to-detector distance of 2.5 m. The samples were mounted in a vacuum chamber, and the incident angles were set at 0.16° or 0.18°, which are above the critical angle (0.135°) of thin films.

Fabrication of the DSSCs

DSSCs were fabricated according to the previously reported procedure.[31–33] Transparent SnO$_2$/F-layered conductive glass (FTO, Pilkington. Co. Ltd., 8 Ω/□) was employed in order to prepare both the photo and counter electrodes. The sol–gel solutions containing the graft copolymer and different amounts of [TTIP]:[H$_2$O]:[HCl] were spin-coated onto the FTO glass and were sintered at 450 °C for 30 min. Then, commercialized TiO$_2$ paste (Ti-Nanoxide T, Solaronix) was cast onto the TiO$_2$ thin film coated FTO glass by a doctor-blade technique, followed by successive sintering at 450 °C for 30 min. The nanocrystalline TiO$_2$ films were sensitized overnight in a Ru(dcbpy)$_2$(NCS)$_2$ dye (dcbpy = 2,2′-bipyridyl-4,4′-dicarboxylato) solution (535-bisTBA, Solaronix, 13 mg, dissolved in 50 g distilled ethanol). Pt-layered counter-electrodes were prepared by spin-coating a 1 wt% H$_2$PtCl$_6$ solution in isopropanol onto the FTO glass and then sintering the film at 450 °C for 30 min. Polymer electrolyte solutions consisting of PEGDME, SiO$_2$, MPII and I$_2$ dissolved in THF were cast onto a dye-adsorbed TiO$_2$ electrode and evaporated very slowly to allow penetration of the electrolytes through the mesopores of the TiO$_2$ layer. The mole ratio of ether oxygen to iodide salt was fixed at 20, and the iodine content was fixed at 10 wt% with respect to the salt.[32,33] Both electrodes were then superposed together and pressed between two glass plates in order to achieve both slow evaporation of the solvent and a thin electrolyte layer. The cells were placed in a vacuum oven for 1 day for complete evaporation of the solvent.

The photoelectrochemical performance, including the short-circuit current (J_{sc}, mA cm^{-2}), open-circuit voltage (V_{oc}, V), fill factor (FF), and overall energy conversion efficiency (η) were measured using a Keithley Model 2400 source meter and a 1000 W xenon lamp (Oriel, 91193). The light was homogeneous up to an 8 × 8 in^2 area and its intensity was calibrated with a Si solar cell (Fraunhofer Institute for Solar Energy System, Mono-Si + KG filter, Certificate No. C-ISE269) for 1 sun light intensity (100 mW cm^{-2}). The intensity was verified with a NREL-calibrated Si solar cell (PV Measurements Inc.). Photo-electrochemical performance was calculated using the following equations:

$$FF = \frac{V_{max} \cdot J_{max}}{V_{oc} \cdot J_{sc}} \quad (1)$$

$$\eta(\%) = \frac{V_{max} \cdot J_{max}}{P_{in}} \times 100 = \frac{V_{oc} \cdot J_{sc} \cdot FF}{P_{in}} \times 100 \quad (2)$$

where J_{sc} is the short-circuit current density (mA cm^{-2}), V_{oc} is the open-circuit voltage (V), P_{in} is the incident light power, and J_{max} (mA cm^{-2}) and V_{max} (V) are the current density and voltage in the J–V curve, respectively, at the point of maximum power output.

Results and discussion

Templated synthesis of organized TiO$_2$ films by graft copolymer

A hydrophilic–hydrophobic microphase-separated graft copolymer is critical for synthesizing well-organized mesoporous TiO$_2$ films. Upon casting using tetrahydrofuran (THF), which is a good solvent for both polymer chains, randomly microphase-separated domains of PVC main chains and POEM side chains with approximately 100 nm of d-spacing were observed without regular patterns (Fig. 1a, b), which is a common morphology for graft copolymers.[34–38] The large difference in the physicochemical properties between the PVC and POEM chains provides the AFM image contrast between the two domains. In phase images, bright regions represent the hydrophobic domains of the glassy PVC main chains whose glass transition temperature (T_g) is 70 °C, whereas dark regions show the hydrophilic, rubbery POEM side chains whose T_g is −58 °C.[33] Upon carefully tuning polymer–solvent interactions using a THF–H$_2$O/HCl mixture, well-organized micelles of the graft copolymer were obtained with a more regular arrayed structure (Fig. 1c, d). Since the THF–H$_2$O/HCl mixture is a poor solvent for the PVC chains, the interfacial energy between the PVC chains and the solvent would be increased, leading to reduced swelling of the PVC main chains and increased stretching of the POEM side chains. As a result, the PVC chains aggregated to form a core of micelles whereas the POEM chains formed a continuous corona outside the core.[39]
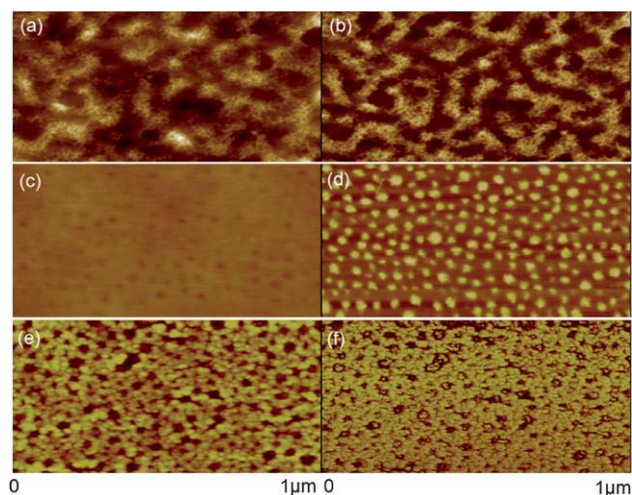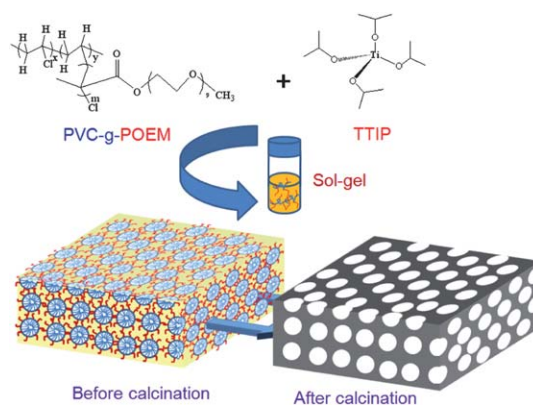
The average sizes of the isolated PVC core in the graft copolymer micelles were estimated to be 32 nm.

The well-organized PVC-g-POEM graft copolymer was used as a structure directing agent to synthesize mesoporous TiO$_2$ films via a sol–gel process using a titanium precursor, i.e., titanium(IV) isopropoxide (TTIP), as represented in Scheme 1. Upon calcination at 450 °C, well-organized mesoporous TiO$_2$ films were obtained with an average pore size of 29 nm (Fig. 1e, f). Strong similarities in the spatial distribution patterns were observed between the well-organized PVC-g-POEM (Fig. 1c, d) and the mesoporous TiO$_2$ film (Fig. 1e, f). This indicates that TTIP is selectively incorporated in the hydrophilic POEM domains, and TiO$_2$ crystallites are formed in situ during calcination, originating from favorable interactions between TTIP and POEM. Moreover, the pore size (29 nm) of the TiO$_2$ film did not greatly differ from that of the PVC core (32 nm) of the well-organized PVC-g-POEM, demonstrating that the graft copolymer functioned as a robust and precise structure-directing agent.

GISAXS has been well established as an experimental technique to complement the structural analysis obtained from the microscopy images because it gives information over a large area.[40–42] Moreover, GISAXS is a versatile tool for correlating nanoscale density within the film and the structure of the film.[40] Although the GISAXS profile overlapped to some degree with the beam stop, a broad shoulder peak at around $q \approx 0.1$ nm^{-1}, which corresponds to the domain spacing of 63 nm, was observed for the organized PVC-g-POEM graft copolymer, indicating a microphase-separated structure (Fig. 2a). Upon combining the organized PVC-g-POEM graft copolymer and the titanium precursor (TTIP) before calcination, a scattering peak centered at 0.128 nm^{-1} appeared, corresponding to a d-spacing of 49 nm (Fig. 2b). After calcination at 450 °C, the scattering peak became more intense and the scattering vector (q) shifted to a lower value at 0.116 nm^{-1} (54 nm), indicating the formation of a more regular structure and the increase of d-spacing in the TiO$_2$ thin films (Fig. 2c).

Characterization of the organized TiO$_2$ interfacial layers

The organized TiO$_2$ films were used as an interfacial layer in DSSCs to increase the energy conversion efficiency. In particular,

Fig. 1 AFM images; (a) height image of PVC-g-POEM prepared from THF, (b) phase image of PVC-g-POEM prepared from THF, (c) height image of PVC-g-POEM prepared from THF–H$_2$O/HCl mixture, (d) phase image of PVC-g-POEM prepared from THF–H$_2$O/HCl mixture, (e) height image of TiO$_2$ film templated by PVC-g-POEM and (f) phase image of TiO$_2$ film templated by PVC-g-POEM. Height was 10 nm and the phase angle was 30°. The mole ratio of [TTIP]:[H$_2$O]:[HCl] was 2 : 0.5 : 0.5.

Scheme 1 Schematic illustration for the synthesis of the organized TiO$_2$ films via the sol–gel process.
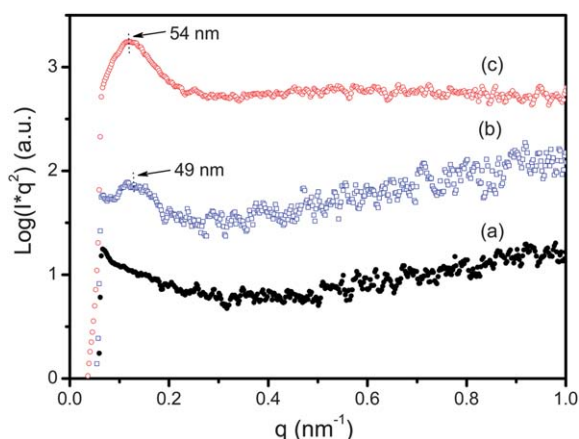
Fig. 2 GISAXS profiles of (a) the organized PVC-g-POEM graft copolymer, the organized TiO$_2$ film templated by the organized PVC-g-POEM (b) before and (c) after calcination at 450 °C. The mole ratio of [TTIP]:[H$_2$O]:[HCl] was 2 : 0.5 : 0.5.

the structure of the TiO$_2$ film was carefully controlled by changing the mole ratio of [TTIP]:[HCl]:[H$_2$O] to investigate the effect of morphology of TiO$_2$ film on the transmittance of FTO glass and interfacial properties. The variation in morphology as a function of the composition of [TTIP]:[HCl]:[H$_2$O] was characterized using SEM, and the results are presented in Fig. 3. A less-organized morphology with a low porosity and a smaller pore size (which is referred to as orgTiO$_2$-1) was obtained at lower water content, i.e., [TTIP]:[HCl]:[H$_2$O] = 2 : 1 : 0 (Fig. 3a), whereas the well-organized morphology with a high porosity and a bigger pore size (orgTiO$_2$-3) was obtained at higher water content, i.e., [TTIP]:[HCl]:[H$_2$O] = 2 : 1 : 1 (Fig. 3c), indicating the importance of water concentration in determining TiO$_2$ morphology. When prepared with [TTIP]:[HCl]:[H$_2$O] = 2 : 0.5 : 0.5 (orgTiO$_2$-2 in Fig. 3b), the morphology of the TiO$_2$ film exhibited an intermediate porosity and pore size, which fell between orgTiO$_2$-1 in Fig. 3a and orgTiO$_2$-3 in Fig. 3c.

Fig. 4 Pictures of TiO$_2$ photoelectrodes; (top) commercial TiO$_2$, (middle) mesoporous TiO$_2$ films at [TTIP]:[HCl]:[H$_2$O] = 2 : 1 : 0, and (bottom) mesoporous TiO$_2$ films at [TTIP]:[HCl]:[H$_2$O] = 2 : 1 : 1.

All the mesoporous TiO$_2$ films were highly transparent irrespective of the composition whereas a randomly oriented TiO$_2$ (Ti-Nanoxide D20, Solaronix) film of a similar thickness was opaque, as seen in Fig. 4. It suggests the homogeneously organized mesoporous structure of TiO$_2$, and provides a direct indication that TTIP grew confined within the POEM domains of the microphase-separated graft copolymer, as presented in Scheme 1.

A 550 nm thick mesoporous TiO$_2$ interfacial layer was deposited as a buffer layer between the FTO and the nanocrystalline TiO$_2$ layer. The nanocrystalline TiO$_2$ layer was coated onto the buffer layer with a thickness of 4 μm using commercial TiO$_2$ paste, as shown in Fig. 5. As shown, good interfacial
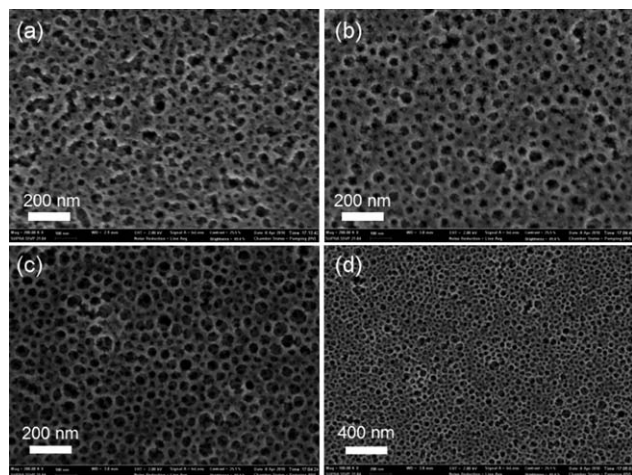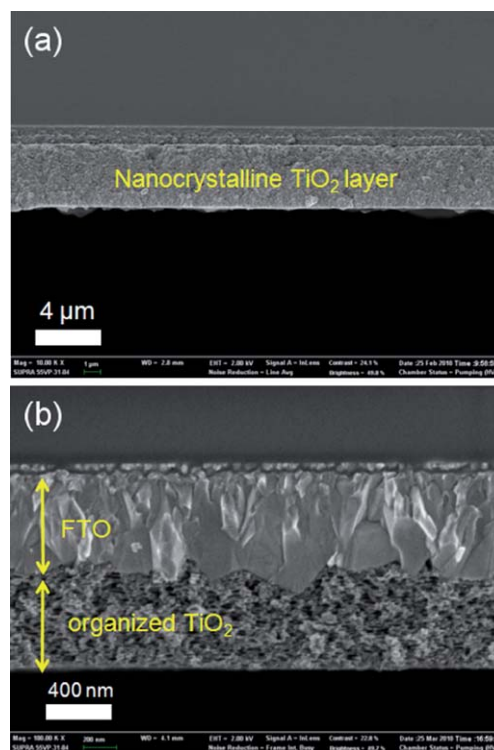

Fig. 3 Plan-view SEM images of organized TiO$_2$ films with different compositions; [TTIP]:[HCl]:[H$_2$O] = (a) 2 : 1 : 0 (which is referred to as orgTiO$_2$-1), (b) 2 : 0.5 : 0.5 (orgTiO$_2$-2) and (c) 2 : 1 : 1 (orgTiO$_2$-3) with high magnification and (d) 2 : 1 : 1 (orgTiO$_2$-2) with low magnification.

Fig. 5 Cross-sectional SEM images of FTO/organized mesoporous TiO$_2$ buffer layer/nanocrystalline TiO$_2$ film; (a) low and (b) high magnification.
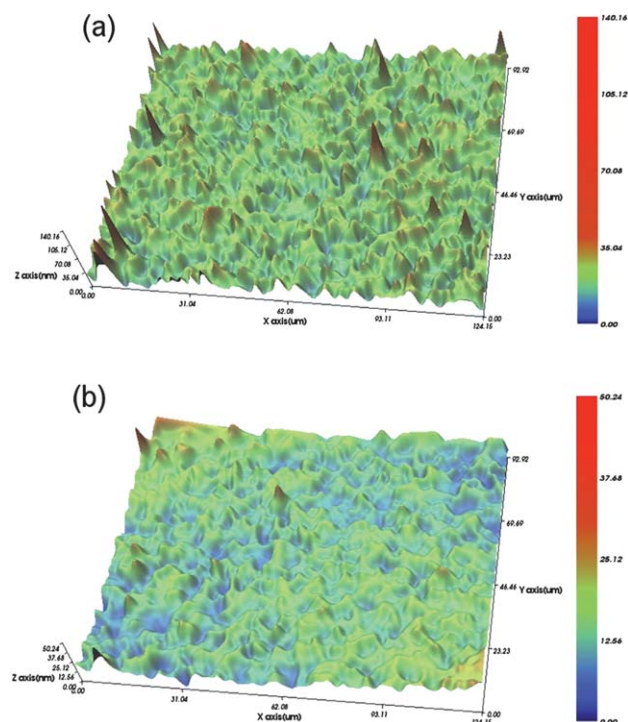
Fig. 6 Noncontact 3D surface profiler SEM images for (a) bare FTO glass and (b) FTO/organized mesoporous TiO_2 layer.

contact between the FTO and mesoporous TiO_2 was achieved. Fig. 6 shows the non-contact 3D surface profiler SEM images for the bare FTO surface and well-organized TiO_2 coated FTO. The root-mean-square roughness of the bare FTO was significantly reduced from 8.4 to 3.2 nm by the deposition of the mesoporous TiO_2 thin film. This result indicates an improvement in interfacial adherence between the mesoporous TiO_2 layer and the TCO, leading to a decreased interfacial resistance.

The transmittance spectra of the bare FTO and the mesoporous TiO_2 coated FTO samples were measured, as shown in Fig. 7. Three kinds of buffer layers were compared: the compact dense buffer layer, the organized TiO_2 layers of orgTiO$_2$-1 in
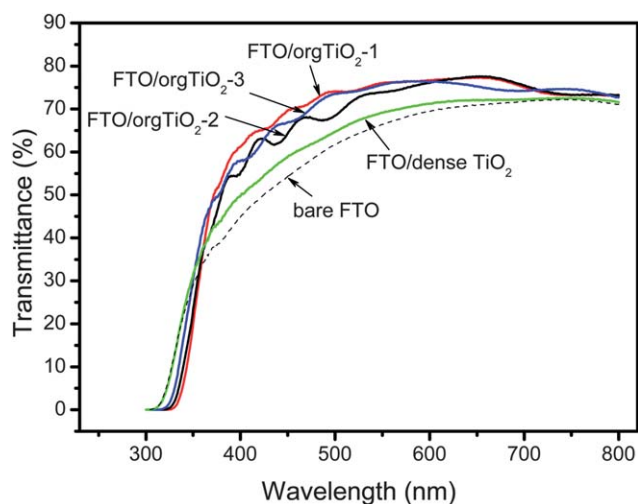

Fig. 7 Transmittance spectra of FTO glasses with and without different buffer layers.

Fig. 3a and orgTiO$_2$-3 in Fig. 3c. The transmittance of the dense TiO_2 layer coated FTO was slightly higher than that of bare FTO glass, probably due to the increased uniformity of the FTO surface. Interestingly, the transmittance of FTO was further increased by the deposition of the organized mesoporous TiO_2 thin films. The orgTiO$_2$-1 coated FTO exhibited slightly higher transmittance than orgTiO$_2$-3 due to the lower porosity of the former as shown in Fig. 3. This antireflective role of the buffer layer on the DSSC performance, especially its influence on the short circuit current (J_{sc}), was investigated using photovoltaic I–V characteristic analysis.

Effect of the organized TiO_2 interfacial layers on DSSC performance

Solid-state DSSCs were fabricated using the organized TiO_2 thin films as an interfacial layer, polymer electrolytes consisting of poly(ethylene glycol dimethyl ether) (PEGDME), fumed silica nanoparticles (SiO_2), 1-methyl-3-propyl imidazolium iodide (MPII) and I_2.[43] The J–V curves of DSSCs with and without the different kinds of buffer layers are presented in Fig. 8, and their photovoltaic parameters are summarized in Table 1. A general trend is the improvement of photocurrent density by the introduction of buffer layer, resulting in the enhancement of energy conversion efficiency irrespective of the kind of buffer layer. For example, the DSSC fabricated without a buffer layer exhibited an efficiency of 3.5% at 100 mW cm^{-2}, which was always increased by the introduction of a buffer layer. In particular, the DSSC
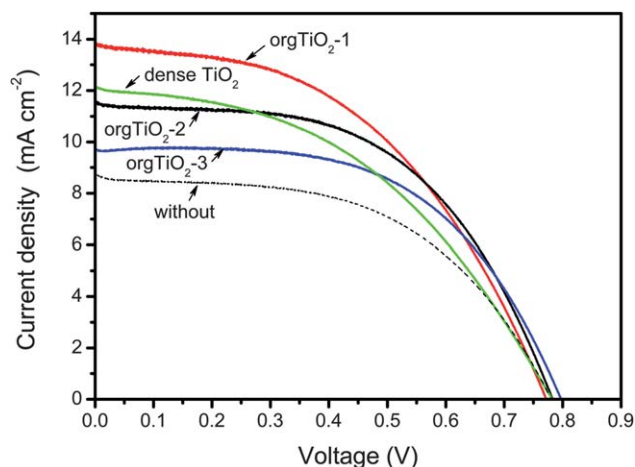

Fig. 8 J–V curves of DSSC employing PEGDME/SiO$_2$/MPII/I$_2$ polymer electrolytes with and without different buffer layers at 100 mW cm^{-2}.

Table 1 Performances of DSSC employing PEGDME/SiO$_2$/MPII/I$_2$ polymer electrolytes with and without different buffer layers at 100 mW cm^{-2}

Buffer layer	V_{oc}/V	J_{sc}/mA cm^{-2}	FF	Efficiency (%)
without	0.78	8.8	0.52	3.5
orgTiO$_2$-1	0.78	13.7	0.47	5.0
orgTiO$_2$-2	0.78	11.6	0.53	4.8
orgTiO$_2$-3	0.80	9.7	0.56	4.3
dense TiO$_2$	0.78	12.2	0.44	4.1

efficiency was enhanced up to 5.0% and 4.3% for the orgTiO$_2$-1 and orgTiO$_2$-3 films, respectively. These improvements are even higher than that achieved using the dense TiO$_2$ film, indicating the importance of mesoporous structure in the interfacial layer. The improved efficiency mostly results from the increase in J_{sc}, which is partially due to the enhanced transmittance of visible light through the FTO glass, as confirmed in Fig. 7. Another possible reason for the efficiency enhancement is the improved interfacial properties between the FTO glass and the nano-crystalline TiO$_2$ layer, which were characterized using EIS analysis. Under the fast electron transfer due to the significant increase of J_{sc}, ion transfer through polymer electrolytes might be limited to some degree, resulting in a slight decrease in fill factor (FF). According to Nogueira's previous work,[44] the low ionic mobility causes the generation of concentration gradients in a polymer electrolyte, especially at high current densities, leading to a decrease in FF.

The efficiency of DSSC also depends strongly on the amount of dye adsorption, which is related, in turn, to the surface area and porosity of the TiO$_2$ photoelectrode. Thus, the dye adsorption of the organized TiO$_2$ thin films were measured by adsorption-desorption experiments.[31,32] The amount of dye adsorption was different depending on the kind of organized TiO$_2$ thin films and arranged in the following order: orgTiO$_2$-3 (12.8 nmol cm^{-2}) $\simeq$ orgTiO$_2$-2 (12.7 nmol cm^{-2}) > orgTiO$_2$-1 (9.8 nmol cm^{-2}). This result is consistent with the porosity and pore size of organized TiO$_2$ film; the lower dye adsorption of orgTiO$_2$-1 film is attributed to a low porosity and a smaller pore size whereas the higher dye adsorption of orgTiO$_2$-3 film is due to a high porosity and a bigger pore size, as confirmed by SEM analysis. However, the DSSC efficiency exhibited the reverse order; orgTiO$_2$-1 (5.0%) > orgTiO$_2$-2 (4.8%) > orgTiO$_2$-3 (4.3%). In addition, the dye adsorption of the organized TiO$_2$ thin films is much smaller than that of nanocrystalline TiO$_2$ thick layer ($\sim$100 nmol cm^{-2}). It is thus concluded that the dye adsorption of the organized mesoporous TiO$_2$ thin films does not contribute to the DSSC performance significantly.

EIS analysis was used to investigate the interfacial properties, internal resistance and charge-transfer kinetics of nanocrystalline TiO$_2$ layers in DSSCs.[45] An applied bias of V_{oc} at a frequency range from 0.01 Hz to 0.1 MHz was used, with an AC amplitude of 0.2 V and a light intensity of 100 mW cm^{-2}. Fig. 9 shows the Nyquist plots, Bode phase plots and equivalent circuit of DSSCs with and without different buffer layers. Electrochemical parameters determined from EIS analysis, i.e., resistance values (R_s, R_1, R_2, and W_s), minimum angular frequency (ω_{min}) and lifetime of electrons for recombination (τ_r), are summarized in Table 2. The impedance spectra can be interpreted and modeled using equivalent circuits, with each component explained below. Each equivalent circuit consisted of several components: ohmic resistance (R_s), charge transfer resistance at the counterelectrode/electrolyte (R_1), charge transfer resistance at the photoelectrode/electrolyte (R_2), resistance at the Warburg diffusion of the redox I$^-$/I$_3^-$ couple in electrolyte (W_s), the constant phase element of capacitance corresponding to R_1 (CPE1), and the constant phase element of capacitance corresponding to R_2 (CPE2).[46] In Fig. 9(a), the Nyquist spectra of the DSSCs showed three semicircles: the first semicircle, in the high-frequency region, represents R_1; the second semicircle, in the middle-frequency region,
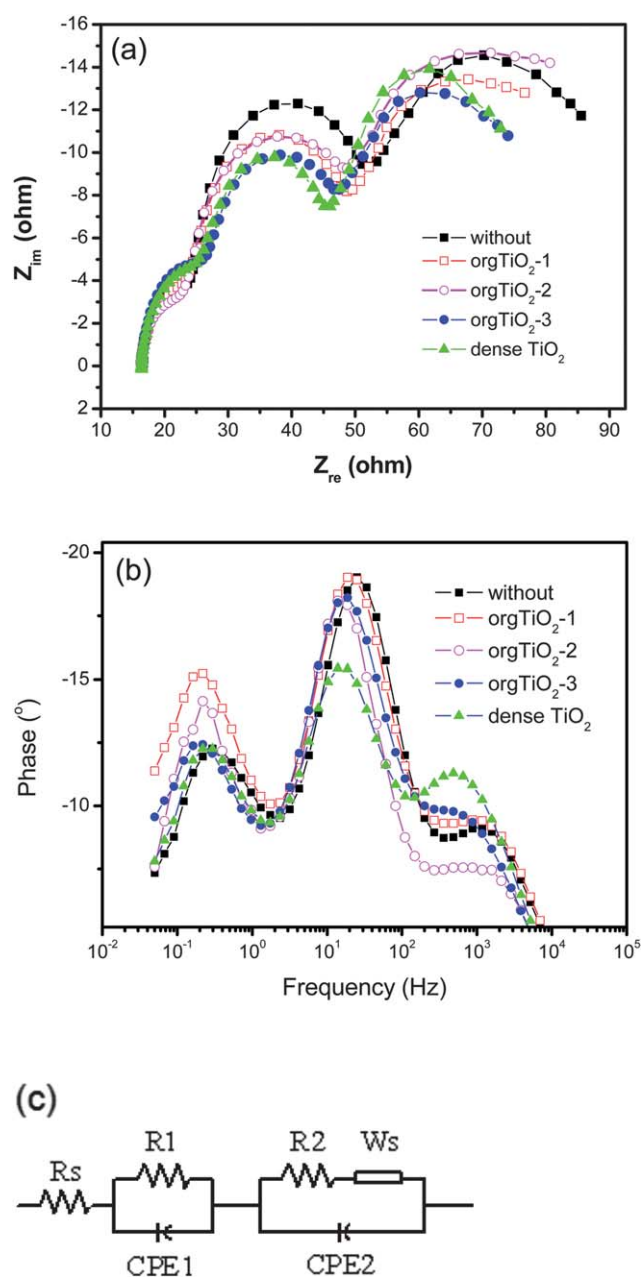

Fig. 9 EIS curves of DSSCs employing PEGDME/SiO$_2$/MPII/I$_2$ polymer electrolytes with and without different buffer layers at 100 mW cm^{-2}; (a) Nyquist plots, (b) Bode plots and (c) equivalent circuit.

Table 2 Electrochemical parameters of DSSC employing PEGDME/SiO$_2$/MPII/I$_2$ polymer electrolytes with and without different buffer layers determined from EIS analysis at 100 mW cm^{-2}

	R_s/Ω	R_1/Ω	R_2/Ω	W_s/Ω	ω_{min}/Hz	τ_r/ms
without	16.4	7.7	28.1	33.3	25.1	39.8
orgTiO$_2$-1	16.3	7.1	25.3	28	13.9	71.9
orgTiO$_2$-2	16.4	7.4	24.9	31.9	13.9	71.9
orgTiO$_2$-3	16.4	8.5	20.3	27.9	18.7	53.5
dense TiO$_2$	16.6	10	20.9	26.5	13.9	71.9

represents R_2; the third semicircle, in the low-frequency region, represents W_s, and the curve from the origin to first semicircle starting point on the left represents R_s. These four internal impedances have a direct effect on the electron transport mechanism in DSSCs. As a consequence, the cell performance of the DSSCs is improved when the sum of the resistance components (R_s, R_1, R_2, and W_s) is small.

As seen in Table 2, both R_s and R_1 of the DSSCs without a buffer layer were not significantly different from those of DSSCs with buffer layers, indicating that the introduction of a buffer layer has little effect on FTO glass resistance and on charge transfer at the counter electrode/electrolyte. However, both R_2 and W_s were decreased by the introduction of the buffer layer, indicating a decrease in charge transfer resistance at the photoelectrode/electrolyte and the resistance related to Warburg diffusion of the I^-/I_3^- redox couple in the electrolyte. In particular, R_2 and W_s decreased from 28.1 Ω to 20.3 Ω and from 33.3 to 27.7 Ω, respectively, when the orgTiO$_2$-3 layer was utilized, indicating the important role of organized TiO$_2$ films in determining the interfacial properties of DSSCs.

According to the EIS model, the lifetime of electrons for recombination (τ_r) in the TiO$_2$ photoelectrode can be estimated from the minimum angular frequency (ω_{min}) value of the impedance semicircle at middle frequencies in the Bode spectrum, according to the relationship: $\tau_r = 1/\omega_{min}$.[47] As seen in Fig. 9b, the middle frequencies in the Bode spectra of DSSCs without a buffer layer shifted to lower frequencies upon the introduction of a buffer layer. As a result, the electron recombination lifetime values (τ_r) for DSSCs were increased by the utilization of the buffer layer. In particular, a τ_r of 39.8 ms for DSSCs without a buffer layer increased up to 71.9 ms when orgTiO$_2$-1 or dense TiO$_2$ films were used. This could effectively decrease electron recombination, leading to significantly enhanced electron transfer and, thus, an improved J_{sc} value. This can also improve adhesion properties between the main nanocrystalline TiO$_2$ layer and FTO that significantly affect the electron transfer or electron recombination at the interface of FTO/TiO$_2$. Therefore, DSSC efficiency could be improved significantly by the introduction of a buffer layer, in particular, the organized TiO$_2$ film.

Conclusions

AFM and GISAXS analysis showed that a randomly microphase-separated graft copolymer was successfully reorganized to show a well-ordered micellar morphology by controlling solvent affinity using a THF–H$_2$O/HCl mixture. Well-organized mesoporous TiO$_2$ films with high porosity and good connectivity were developed *via* the sol–gel process using an organized PVC-*g*-POEM amphiphilic graft copolymer. In particular, organized TiO$_2$ thin films with different morphologies were prepared by carefully changing the mole ratio of [TTIP]:[H$_2$O]:[HCl]. A organized TiO$_2$ film with a lower porosity and smaller pore size (orgTiO$_2$-1) was obtained at a lower water content, *i.e.* [TTIP]:[HCl]:[H$_2$O] = 2 : 1 : 0, whereas the TiO$_2$ film with a higher porosity and bigger pores (orgTiO$_2$-3) was prepared at higher water content, *i.e.*, [TTIP]:[HCl]:[H$_2$O] = 2 : 1 : 1. The organized TiO$_2$ thin films were used as an interfacial layer in DSSCs, and the influence of the material structure on photovoltaic performance was then investigated. The root-mean-square roughness of the FTO substrate was dramatically reduced from 8.4 to 3.2 nm by the deposition of mesoporous TiO$_2$ thin films, indicating an improvement in interfacial adherence between the mesoporous TiO$_2$ layer and TCO, as confirmed by noncontact 3D surface profiler SEM images. By introducing the organized TiO$_2$ thin films as an interfacial layer in DSSCs, J_{sc} significantly increased from 8.8 up to 13.7 mA cm^{-2}, thus improving the photovoltaic conversion efficiency from 3.5% up to 5.0%, at 100 mW cm^{-2} for solid-state DSSCs employing PEGDME/SiO$_2$/MPII/I$_2$ polymer electrolytes. EIS analysis showed that the interfacial resistance of the DSSC with the orgTiO$_2$-3 film was smaller than that with the orgTiO$_2$-1, but the electron recombination lifetime of the former was shorter than the latter. Moreover, the antireflective capability of the orgTiO$_2$-1 thin film was slightly higher than that of the orgTiO$_2$-3 film. As a result, the efficiency of the DSSC fabricated with the orgTiO$_2$-1 thin film as an interfacial layer was higher than that with the orgTiO$_2$-3 film, indicating the importance of the morphology of the organized TiO$_2$ thin film.

References

1 B. O'Regan and M. Gratzel, *Nature*, 1991, **353**, 737.
2 C.-Y. Chen, J.-G. Chen, S.-J. Wu, J.-Y. Li, C.-G. Wu and K.-C. Ho, *Angew. Chem., Int. Ed.*, 2008, **47**, 7342.
3 P. Wang, S. M. Zakeeruddin, J. E. Moser, M. K. Nazeeruddin, T. Sekiguchi and M. Gratzel, *Nat. Mater.*, 2003, **2**, 402.
4 J. R. Jennings, A. Ghicov, L. M. Peter, P. Schmuki and A. B. Walker, *J. Am. Chem. Soc.*, 2008, **130**, 13364.
5 S. Yanagida, Y. Yu and K. Manseki, *Acc. Chem. Res.*, 2009, **42**, 1827.
6 B. Yoo, K. Kim, D. K. Lee, M. J. Ko, H. Lee, Y. H. Kim, W. M. Kim and N. G. Park, *J. Mater. Chem.*, 2010, **20**, 4392.
7 J. E. Benedetti, M. A. de Paoli and A. F. Nogueira, *Chem. Commun.*, 2008, 1121.
8 J. Xia, N. Masaki, M. Lira-Cantu, Y. Kim, K. Jiang and S. Yanagida, *J. Am. Chem. Soc.*, 2008, **130**, 1258.
9 R. Zhu, C.-Y. Jiang, B. Liu and S. Ramakrishna, *Adv. Mater.*, 2009, **21**, 994.
10 K. C. Huang, Y. C. Wang, R. X. Dong, W. C. Tsai, K. W. Tsai, C. C. Wang, Y. H. Chen, R. Vittal, J. J. Lin and K. C. Ho, *J. Mater. Chem.*, 2010, **20**, 4067.
11 J. N. de Freitas, A. F. Nogueira and M. A. De Paoli, *J. Mater. Chem.*, 2009, **19**, 5279.
12 H. W. Han, W. Liu, J. Zhang and X.-Z. Zhao, *Adv. Funct. Mater.*, 2005, **15**, 1940.
13 S. Wu, H. Han, Q. Tai, J. Zhang, S. Xu, C. Zhou, Y. Yang, H. Hu, B. Chen and X.-z. Zhao, *J. Power Sources*, 2008, **182**, 119.
14 T. Stergiopoulos, A. Valota, V. Likodimos, T. Speliotis, D. Niarchos, P. Skeldon, G. E. Thompson and P. Falaras, *Nanotechnology*, 2009, **20**, 365601.
15 G. K. R. Senadeera, T. Kitamura, Y. Wada and S. Yanagida, *J. Photochem. Photobiol., A*, 2006, **184**, 234.
16 J. Jiu, F. Wang, M. Sakamoto, J. Takao and M. Adachi, *Sol. Energy Mater. Sol. Cells*, 2005, **87**, 77.
17 L. Kavan and M. Grätzel, *Electrochim. Acta*, 1995, **40**, 643.

18 S. Ito, P. Liska, P. Comte, R. Charvet, P. Péchy, U. Bach, L. Schmidt-Mende, S. M. Zakeeruddin, A. Kay, M. K. Nazeeruddin and M. Grätzel, *Chem. Commun.*, 2005, 4351.

19 J. Xia, N. Masaki, K. Jiang and S. Yanagida, *J. Phys. Chem. B*, 2006, **110**, 25222.

20 Y.-Q. Wang, S.-G. Chen, X.-H. Tang, O. Palchik, A. Zaban, Y. Koltypin and A. Gedanken, *J. Mater. Chem.*, 2001, **11**, 521.

21 K. Hou, B. Tian, F. Li, Z. Bian, D. Zhao and C. Huang, *J. Mater. Chem.*, 2005, **15**, 2414.

22 K. S. Ahn, M. S. Kang, J. W. Lee and Y. S. Kang, *J. Appl. Phys.*, 2007, **101**, 084312.

23 Y. J. Kim, Y. H. Lee, M. H. Lee, H. J. Kim, J. H. Pan, G. I. Lim, Y. S. Choi, K. Kim, N.-G. Park, C. Lee and W. I. Lee, *Langmuir*, 2008, **24**, 13225.

24 K. M. Coakley, Y. X. Liu, M. D. McGehee, K. L. Frindell and G. D. Stucky, *Adv. Funct. Mater.*, 2003, **13**, 301.

25 M. Zukalová, A. Zukal, L. Kavan, M. K. Nazeeruddin, P. Liska and M. Grätzel, *Nano Lett.*, 2005, **5**, 1789.

26 Y.-J. Cheng and J. S. Gutmann, *J. Am. Chem. Soc.*, 2006, **128**, 4658.

27 Z. C. Sun, D. H. Kim, M. Wolkenhauer, G. G. Bumbu, W. Knoll and J. S. Gutmann, *ChemPhysChem*, 2006, **7**, 370.

28 M. Nedelcu, J. Lee, E. J. W. Crossland, S. C. Warren, M. C. Orilall, S. Guldin, S. Huttner, C. Ducati, D. Eder, U. Wiesner, U. Steiner and H. J. Snaith, *Soft Matter*, 2009, **5**, 134.

29 L. Chen, B. Yao, Y. Cao and K. Fan, *J. Phys. Chem. C*, 2007, **111**, 11849.

30 H.-S. Yun, K. Miyazawa, H. S. Zhou, I. Honma and M. Kuwabara, *Adv. Mater.*, 2001, **13**, 1377.

31 S. H. Ahn, J. H. Koh, J. A. Seo and J. H. Kim, *Chem. Commun.*, 2010, **46**, 1935.

32 J. T. Park, D. K. Roh, R. Patel, E. Kim, D. Y. Ryu and J. H. Kim, *J. Mater. Chem.*, 2010, **20**, 8521.

33 D. K. Roh, J. T. Park, S. H. Ahn, H. Ahn, D. Y. Ryu and J. H. Kim, *Electrochim. Acta*, 2010, **55**, 4976.

34 M. Zhang and T. P. Russell, *Macromolecules*, 2006, **39**, 3531.

35 K. J. Lee, J. T. Park, J. H. Goh and J. H. Kim, *J. Polym. Sci., Part A: Polym. Chem.*, 2008, **46**, 3911.

36 J. F. Hester, P. Banerjee, Y. Y. Won, A. Akthakul, M. H. Acar and A. M. Mayes, *Macromolecules*, 2002, **35**, 7652.

37 Y. W. Kim, J. K. Choi, J. T. Park and J. H. Kim, *J. Membr. Sci.*, 2008, **313**, 315.

38 N. Bicak and M. Ozlem, *J. Polym. Sci., Part A: Polym. Chem.*, 2003, **41**, 3457.

39 P. C. A. Alberius, K. L. Frindell, R. C. Hayward, E. J. Kramer, G. D. Stucky and B. F. Chmelka, *Chem. Mater.*, 2002, **14**, 3284.

40 Z. Sun, D. H. Kim, M. Wolkenhauer, G. G. Bumbu, W. Knoll and J. S. Gutmann, *ChemPhysChem*, 2006, **7**, 370.

41 E. Martinelli, S. Menghetti, G. Galli, A. Glisenti, S. Krishnan, M. Y. Paik, C. K. Ober, D. M. Smilgies and D. A. Fischer, *J. Polym. Sci., Part A: Polym. Chem.*, 2009, **47**, 267.

42 J. Perlich, M. Memesa, A. Diethert, E. Metwalli, W. Wang, S. V. Roth, A. Timmann, J. S. Gutmann and P. Muller-Buschbauma, *ChemPhysChem*, 2009, **10**, 799.

43 J. H. Kim, M. S. Kang, Y. J. Kim, J. Won, N. G. Park and Y. S. Kang, *Chem. Commun.*, 2004, 1662.

44 A. F. Nogueira, M.-A. De Paoli, I. Montanari, R. Monkhouse, J. Nelson and J. R. Durrant, *J. Phys. Chem. B*, 2001, **105**, 7517.

45 P.-Y. Chen, C.-P. Lee, R. Vittal and K.-C. Ho, *J. Power Sources*, 2010, **195**, 3933.

46 L. Y. Han, N. Koide, Y. Chiba and T. Mitate, *Appl. Phys. Lett.*, 2004, **84**, 2433.

47 R. Kern, R. Sastrawan, J. Ferber, R. Stangl and J. Luther, *Electrochim. Acta*, 2002, **47**, 4213.

This journal is © The Royal Society of Chemistry 2011

J. Mater. Chem., 2011, **21**, 1772–1779 | 1779